
# Tissint Martian Meteorite: A Fresh Look at the Interior, Surface, and Atmosphere of Mars

H. Chennaoui Aoudjehane *et al.*

*Science* **338**, 785 (2012);
DOI: 10.1126/science.1224514

stages of oxidation and show the conversion of the less stable macrocycles into the knot, which is presumably the smallest oligomer that can maximize hydrophobic stabilization. Although other pathways may be involved, the kinetic profile shown in Fig. 3 suggests that knot formation predominantly occurs via the formation and folding of the open trimer. Once formed, the open trimer folds into condensed structures that bury the hydrophobic NDI surfaces. Presumably only one of the structures places the terminal thiols in sufficiently close proximity to allow the ring closure that results in a knot. If the ring were opened by cleavage of a disulfide link, closure would be rapid, whereas unfolding would require unfavorable and slow reexposure of hydrophobic surfaces. The formation of the trefoil knot is, therefore, kinetically and thermodynamically favored and closely mimics the mechanism of knot formation in naturally occurring α/β methyl transferases (*18*).

The conclusions drawn from the experimental results were corroborated by molecular modeling calculations, which showed that the knot was relatively more stable and has a smaller surface area and volume than its topological isomers (the closed trimer and the [2]catenane) (*19*).

Although the cyclic monomer and dimer are transiently formed in the library, the reversible nature of the disulfide bond allows their reorganization into the more ordered, but more stable, trimeric knot, highlighting the dual conflicting role of entropy at the different stages of the folding process: On one hand, the formation of small molecules is preferred, whereas the formation and stability of the larger knot result from the necessity of burying hydrophobic surfaces. Overall, the design of the building block offers an efficient way to access purely organic knotted macrocycles in aqueous media. First, the alternation of rigid hydrophobic NDIs, which can stack and form the core of the knot and bury most hydrophobic surfaces, and flexible hydrophilic loops supplies an ideal scaffold for the knitting of organic oligomers into complex knots. Second, the choice of the amino acid chirality is crucial: The all-L and all-D building blocks induce the directionality of the knot; whereas in the D/L building block, the mismatch of chiralities prevents knot formation. The folding of a linear species into a knot, driven by the hydrophobic effect, may provide a simple model for the formation of knots in proteins.

### References and Notes


1. L. F. Liu, L. Perkocha, R. Calendar, J. C. Wang, *Proc. Natl. Acad. Sci. U.S.A.* **78**, 5498 (1981).
2. C. Z. Liang, K. Mislow, *J. Am. Chem. Soc.* **116**, 11189 (1994).
3. P. Virnau, A. L. Mallam, S. E. Jackson, *J. Phys. Condens. Matter* **23**, 033101 (2011).
4. J.-P. Sauvage, D. B. Amabilino, *Supramol. Chem.* (2012).
5. J. Guo, P. C. Mayers, G. A. Breault, C. A. Hunter, *Nat. Chem.* **2**, 218 (2010).
6. C. O. Dietrich-Buchecker, J.-P. Sauvage, *Angew. Chem. Int. Ed. Engl.* **28**, 189 (1989).
7. J.-F. Ayme *et al.*, *Nat. Chem.* **4**, 15 (2012).
8. P. E. Barran *et al.*, *Angew. Chem. Int. Ed. Engl.* **50**, 12280 (2011).
9. K. I. Arias, E. Zysman-Colman, J. C. Loren, A. Linden, J. S. Siegel, *Chem. Commun. (Camb.)* **47**, 9588 (2011).
10. L.-E. Perret-Aebi, A. von Zelewsky, C. Dietrich-Buchecker, J.-P. Sauvage, *Angew. Chem. Int. Ed.* **43**, 4482 (2004).
11. O. Safarowsky, M. Nieger, R. Fröhlich, F. Vögtle, *Angew. Chem. Int. Ed. Engl.* **39**, 1616 (2000).
12. M. Feigel, R. Ladberg, S. Engels, R. Herbst-Irmer, R. Fröhlich, *Angew. Chem. Int. Ed.* **45**, 5698 (2006).
13. P. T. Corbett *et al.*, *Chem. Rev.* **106**, 3652 (2006).
14. S. Wallin, K. B. Zeldovich, E. I. Shakhnovich, *J. Mol. Biol.* **368**, 884 (2007).
15. F. B. L. Cougnon, N. A. Jenkins, G. D. Pantoş, J. K. M. Sanders, *Angew. Chem. Int. Ed. Engl.* **51**, 1443 (2012).
16. N. Ponnuswamy, G. D. Pantoş, M. M. J. Smulders, J. K. M. Sanders, *J. Am. Chem. Soc.* **134**, 566 (2012).
17. S. Anderson, H. L. Anderson, J. K. M. Sanders, *Acc. Chem. Res.* **26**, 469 (1993).
18. A. L. Mallam, E. R. Morris, S. E. Jackson, *Proc. Natl. Acad. Sci. U.S.A.* **105**, 18740 (2008).
19. The lower stability of the cyclic monomer and dimer was apparent when, during our attempt to isolate these macrocycles, they rapidly reequilibrated into a library dominated by the knot.
20. J. J. P. Stewart, *J. Mol. Model.* **13**, 1173 (2007).
21. M. Korth, *J. Chem. Theory Comput.* **6**, 3808 (2010).
22. A. Klamt, G. Schüürmann, *J. Chem. Soc., Perkin Trans. 2* **2**, 799 (1993).


**Acknowledgments:** We are grateful to Gates Cambridge (N.P.), Engineering and Physical Sciences Research Council (F.B.L.C., J.K.M.S.), and the University of Bath (G.D.P.) for financial support. We thank S. Jackson for helpful discussions, N. Jenkins for his contribution in the early stage on the project, and A. Belenguer for maintaining the LC-MS facility.

### Supplementary Materials

www.sciencemag.org/cgi/content/full/338/6108/783/DC1
Materials and Methods
Figs. S1 to S22
Tables S1 to S4
References

5 July 2012; accepted 11 September 2012
10.1126/science.1227032

# Tissint Martian Meteorite: A Fresh Look at the Interior, Surface, and Atmosphere of Mars

H. Chennaoui Aoudjehane,[1,2]* G. Avice,[3] J.-A. Barrat,[4] O. Boudouma,[2] G. Chen,[5] M. J .M. Duke,[6] I. A. Franchi,[7] J. Gattacceca,[8] M. M Grady,[7,9] R. C. Greenwood,[7] C. D. K. Herd,[5] R. Hewins,[10] A. Jambon,[2] B. Marty,[3] P. Rochette,[8] C. L Smith,[9,11,12] V. Sautter,[10] A. Verchovsky,[7] P. Weber,[13] B. Zanda[10]

Tissint (Morocco) is the fifth martian meteorite collected after it was witnessed falling to Earth. Our integrated mineralogical, petrological, and geochemical study shows that it is a depleted picritic shergottite similar to EETA79001A. Highly magnesian olivine and abundant glass containing martian atmosphere are present in Tissint. Refractory trace element, sulfur, and fluorine data for the matrix and glass veins in the meteorite indicate the presence of a martian surface component. Thus, the influence of in situ martian weathering can be unambiguously distinguished from terrestrial contamination in this meteorite. Martian weathering features in Tissint are compatible with the results of spacecraft observations of Mars. Tissint has a cosmic-ray exposure age of 0.7 ± 0.3 million years, consistent with those of many other shergottites, notably EETA79001, suggesting that they were ejected from Mars during the same event.

Demonstration in the early 1980s that an important group of meteorites was of martian origin represented a breakthrough in attempts to understand the geological evolution of Mars (*1*–*3*). Unfortunately, most of the samples were collected long after their arrival on Earth and thus have experienced variable degrees of terrestrial weathering (*4*). Even the few martian meteorites that were collected shortly after their observed fall to Earth have been exposed to organic and other potential contaminants during storage. Here, we report on the Tissint martian meteorite, which fell on 18 July 2011 in Morocco (figs. S1 and S2). This is only the fifth witnessed fall of a meteorite from Mars and therefore provides an opportunity to improve our understanding of processes that operated on that planet at the time the meteorite was ejected from its surface.

The largest recovered stones from the Tissint fall are almost fully covered with a shiny black fusion crust (Fig. 1). Internally the meteorite consists of olivine macrocrysts set in a fine-grained matrix of pyroxene and feldspathic glass (maskelynite) (*5*) (figs. S3 to S6 and tables S1 to S6). The matrix is highly fractured and penetrated by numerous dark shock veins and patches filled with black glassy material enclosing bubbles (fig. S7). The petrology of Tissint shows similarities to that of other picritic shergottites (an important group of olivine-rich martian basaltic rocks), in particular, lithologies A and C of EETA79001 (*2*). The grain density and magnetic properties of Tissint (fig. S8) also match previous results from basaltic and picritic shergottites (*6*).

Tissint is an Al-poor ferroan basaltic rock, rich in MgO and other compatible elements (Ni,

Cr, Co). Its major element abundances are similar to those of the other picritic shergottites, especially EETA79001. Furthermore, key element weight (wt) ratios (wt %/wt %) such as FeO/MnO (39.7), Al/Ti (7.2), Na/Ti (1.41), Ga/Al (3.9 $10^{-3}$), Na/Al (0.20) (*3*, *4*, *7*), and $\Delta^{17}O$ [+0.301 per mil (‰)] (fig. S9) (*8*) are also typical of martian meteorites. The average composition of the black glass (tables S7 and S8) is identical to a mixture of the major phases of the rock (augite, maskelynite, and olivine: 50:20:30) with compositional variations reflecting incomplete dissolution of one phase or another (fig. S7). Among minor elements in the black glass, chlorine is always below the detection level of electron microprobe analysis [100 parts per million (ppm)], whereas fluorine and sulfur exhibit variations in the range 0 to 4000 ppm and 0 to 6000 ppm, respectively (*5*).

Like most other picritic shergottites, bulk Tissint displays a marked depletion in light rare earth elements (LREEs) and other highly incompatible elements, such as Rb, Li, Be, Nb, Ta, Th, and U (Fig. 2). Its Lu/Hf ratio (0.2) is in the range of values measured for EETA79001 and other basaltic shergottites [0.1 to 0.2; e.g., (*9*)], and lower than those of the picritic shergottites DaG 476/489, SaU 005, and Dhofar 019 [about 0.3 (*10*–*12*)]. Although the sizes of the two samples analyzed here are somewhat limited (0.49 and 1.25 g), their trace-element abundances are very similar and so are likely to be representative of the whole rock composition, despite the irregular distribution of olivine megacrysts.

To evaluate the possible heterogeneity of this stone, we analyzed two additional samples: a groundmass-rich sample (devoid of large olivine crystals and weighing 181 mg) and a fragment of the same glassy pocket selected for volatile analysis (40 mg). Both samples display markedly higher LREE abundances, with REE patterns generally similar to those of the enriched shergottites, as exemplified by Zagami. However, there is a minor, but analytically valid, positive Ce anomaly (Ce/Ce* = 1.1) (Fig. 2), and the La/Nd, La/Nb, and Th/La ratios are higher than those of other enriched shergottites (fig. S10). These two samples indicate that an LREE-enriched component, different from those previously recorded in other shergottites, is heterogeneously dispersed throughout the matrix of Tissint.

The presence of short-lived $^{48}V$ (half-life = 16 days), among other cosmogenic isotopes, demonstrates that the stones we analyzed are from the fall of 18 July (table S10). We measured stable cosmogenic isotopes of He, Ne, and Ar in three aliquots, consisting of matrix-rich, glass-matrix mixed, and glass-rich separates (table S11). The cosmic-ray exposure (CRE) ages computed for $^{3}He_c$, $^{21}Ne_c$, and $^{38}Ar_c$ are 1.2 ± 0.4, 0.6 ± 0.2, and 0.9 ± 0.4 million years (My), respectively, resulting in an average CRE age of 0.7 ± 0.3 My for Tissint. This age is in the range of CRE ages of other shergottites, notably that of EETA79001 [0.73 ± 0.15 My (*2*)], suggesting that Tissint and other shergottites were ejected during a single event. Nitrogen isotopes were analyzed together with the noble gases. The glass aliquot displayed a well-defined excess of $^{15}N$, which persisted after correction for contribution of cosmogenic $^{15}N_c$ (assuming a production rate of 6.7 ± 2.6 × $10^{-13}$ mol $^{15}N$/gMa) (*13*). This excess $^{15}N$ is best explained by trapping of a martian atmospheric component (*2*). Using a $\delta^{15}N$ versus $^{40}Ar/N$ correlation and taking a martian atmospheric value from the Viking measurements of 0.33 ± 0.03 (*14*), we obtain a $\delta^{15}N$ value of 634 ± 60‰ (1σ), which agrees well with the Viking measurement of 620 ± 160‰ (*7*) (Fig. 3).

Simultaneous measurement of carbon and nitrogen was carried out by stepped combustion–mass spectrometry on a small chip (21 mg) from the same sample that we used for oxygen isotopic analysis (*5*). The sample had a total carbon abundance of 173 ppm and $\delta^{13}C$ of –26.6 ‰ and contained 12.7 ppm nitrogen with total $\delta^{15}N$ of –4.5‰. At temperatures above 600°C, both carbon and nitrogen were distributed among three discrete martian components (fig. S11 and table S12). Below 600°C, readily resolvable components of organic material combusted; although these may have been introduced during postfall collection and sample storage and are an unavoidable consequence of sample handling procedures, we cannot yet rule out the presence of small quantities of indigenous martian organic matter (*5*). At the highest temperatures of the extraction, there was a clear indication of the presence of trapped martian atmosphere, with elevated $\delta^{13}C$ and $\delta^{15}N$ (even allowing for a cosmogenic component, blank-corrected $\delta^{13}C$ reaches +16‰ and $\delta^{15}N$ reaches +298 ± 25‰). At intermediate temperatures (600° to 800°C), there were maxima in both $\delta^{13}C$ (–14‰) and $\delta^{15}N$ (+110‰), suggesting that the component bears some relationship to the martian atmosphere. In addition, there was clear analytical evidence for a simultaneous release of sulfur (~19 ppm), presumably from either sulfide or sulfate decomposition. This intermediate component probably corresponds to a surface-derived weathering component, as identified in Tissint glass on the basis of REE, S, and


**Fig. 1.** The Natural History Museum (London) stone. This 1.1-kg stone (BM.2012,M1) exhibits a black fusion crust with glossy olivines. The olivine macrocrysts (pale green) and the numerous black glass pockets and veins are characteristics of this shergottite. The scale is in centimeters.

[1]Hassan II University Casablanca, Faculty of Sciences, Géosciences Appliquées à l'Ingénierie et l'Aménagement (GAIA) Laboratory, BP 5366 Maârif, Casablanca Morocco. [2]Université Pierre et Marie Curie Paris 6, Institut de la Terre de Paris (UMR 7193) 4 Place Jussieu, 75005 Paris France. [3]Centre de Recherches Pétrographiques et Géochimiques-CNRS, Université de Lorraine, 15 rue Notre Dame des Pauvres, BP 20, F-54501 Vandoeuvre-lès-Nancy, France. [4]Université de Bretagne Occidentale–Institut Universitaire Européen de la Mer, UMR 6538, Place Nicolas Copernic, 29280 Plouzané Cedex, France. [5]Department of Earth and Atmospheric Sciences, University of Alberta, Edmonton, AB, T6G 2E3, Canada. [6]SLOWPOKE Nuclear Reactor Facility, 1-20 University Hall, University of Alberta, Edmonton, AB, T6G 2J9, Canada. [7]Planetary and Space Sciences, The Open University, Walton Hall, Milton Keynes, MK7 6AA, UK. [8]Centre Européen de Recherche et d'Enseignement des Géosciences de l'Environnement, CNRS Aix-Marseille University, BP80 13545 Aix en Provence, Cedex 4, France. [9]Department of Mineralogy, Natural History Museum, Cromwell Road London SW7 5BD, UK. [10]Laboratoire d'Etudes de la Matière Extraterrestre, Muséum National d'Histoire Naturelle and CNRS-UMS2679, 61 rue Buffon, 75005 Paris, France. [11]ESA (European Space Agency) European Space Research and Technology Center, Keplerlaan 1, 2200 AG Noordwijk, Netherlands. [12]UK Space Agency, ESA Harwell Centre, Atlas Building, Harwell Oxford, Didcot, Oxfordshire OX11 0QX, UK. [13]University of Bern, Albert Einstein Center for Fundamental Physics, Sidlerstrasse 5, CH-3012 Bern, Switzerland.

*To whom correspondence should be addressed. E-mail: chennaoui_h@yahoo.fr, h.chennaoui@fsac.ac.ma

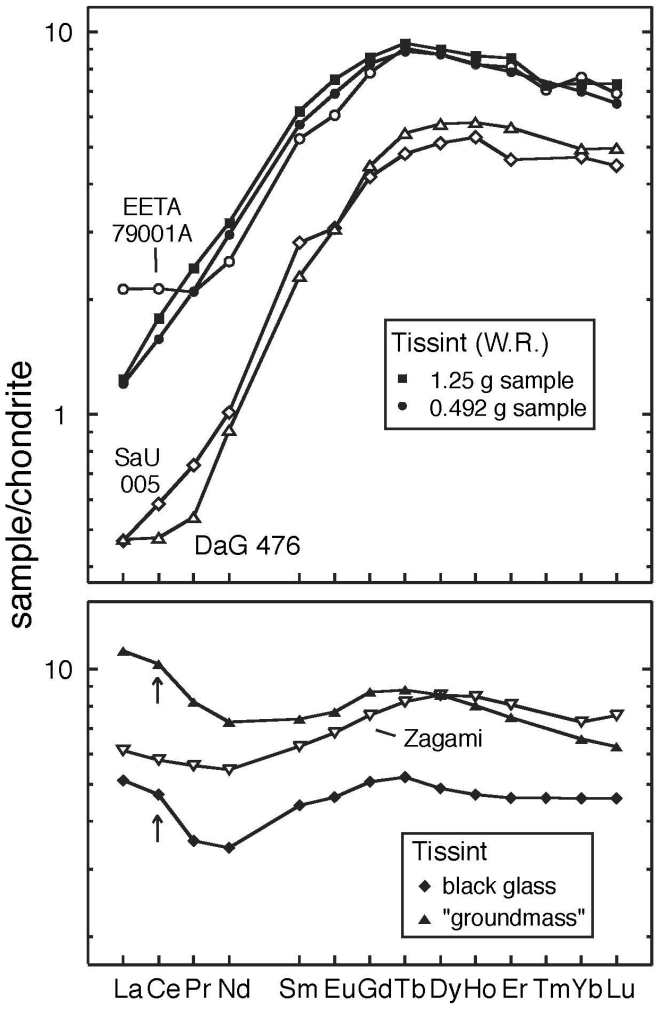


**Fig. 2.** REE patterns. (**Top**) Tissint in comparison with other depleted picritic shergottites. (**Bottom**) Black glass and groundmass-rich fraction in comparison with enriched shergottite Zagami. Data from (*10*–*12*). CI chondrite normalization values are from (*24*).

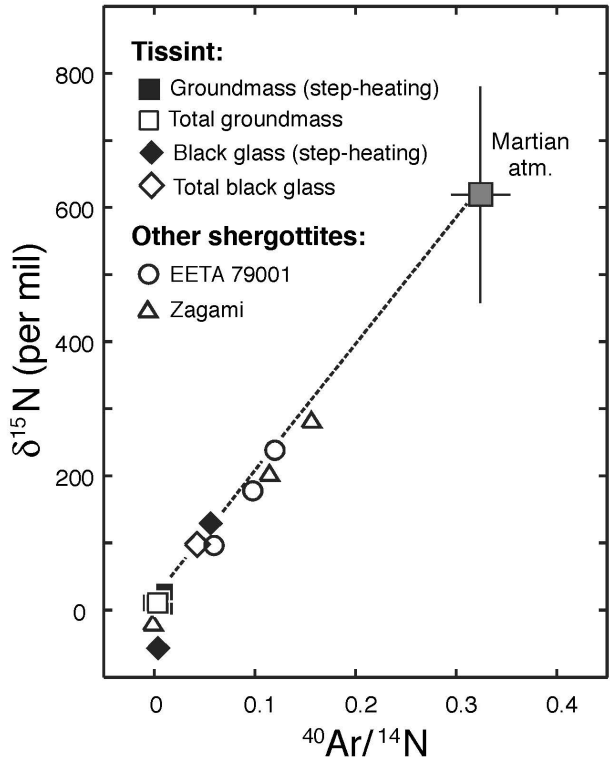


**Fig. 3.** Gas analyses of the black glass. Both bulk analyses and step-heating analyses plot on a single mixing line between terrestrial atmospheric gas (at left) and Mars atmospheric gas (*14*). Zagami data from (*25*).

F data (see below). The third martian component represents magmatic carbon, which is present in low abundance (1.4 ppm with $\delta^{13}C$ of –26.3‰) and is associated with isotopically light nitrogen ($\delta^{15}N < +10‰$).

Our study demonstrates that Tissint is a picritic shergottite comparable in many respects to EETA79001. The black shock glass resembles lithology C of EETA79001, as well as shock melt pockets commonly found in other shergottites (*15*). Major elements and oxygen isotope data indicate that this glass represents a melted mixture of the surrounding bulk rock, composed of olivine, maskelynite, and clinopyroxene (*5*). However, this glass is substantially different from the bulk meteorite and igneous groundmass in that it has a variable but generally high S and F content; a distinct LREE-enriched composition; and a high $\delta^{15}N$ value indicative of trapped martian atmosphere.

The LREE-enriched composition of the glass is somewhat enigmatic. Phosphates are often invoked as a carrier of REE. However, the P content of the black glass relative to bulk rock is not consistent with enrichment in phosphates. One possibility to explain the LREE composition of the glass might be selective crustal contamination before final emplacement of the Tissint magma. Although LREE-enriched magmatic rocks have been generated on Mars, as exemplified by the Nakhlites and Chassignites, these do not exhibit anomalous Ce abundances (*16*, *17*). In addition, crustal contamination of magma is unlikely to result in REE ratio variations at the subcentimeter scale, as observed here. Decoupling of Ce from the other REE indicates partial oxidation to $Ce^{4+}$, a process that requires oxidizing conditions, such as those that prevail in the near-surface environment of Mars. Surface weathering caused by leaching of phosphates by acid aqueous fluids, the process that is responsible for terrestrial alteration of eucritic meteorites in Antarctica (*18*), would also explain the LREE-enriched composition of the Tissint glass. The high $\delta^{15}N$ value of the Tissint glass, as well as its enrichment in S and F, demonstrates that it has been contaminated by martian surface components. In view of this evidence, the most likely explanation for the relatively LREE-enriched composition of the glass, and the origin of the Ce anomaly, is that these features also reflect the presence of a near-surface martian component in Tissint. A martian soil component was previously suggested for EETA79001 lithology C, which also contains martian atmospheric gases (*19*). However, because this meteorite is a find, rather than a fresh fall like Tissint, there's the possibility of terrestrial contamination, which complicates the interpretation (*20*).

We propose the following scenario to explain the composite nature of Tissint. A picritic basalt was emplaced at or near the surface of Mars. After some period, the rock was weathered by fluids, which had leached elements from the martian regolith. Subsequently, these fluids

deposited mineral phases within fissures and cracks. The martian weathering products are the most likely source of the required LREE, incompatible, and volatile elements. Upon impact, preferential, shock-induced melting occurred in the target rock along fractures where weathering products were concentrated. This melting produced the black glass and retained in it chemical signatures characteristic of the martian surface. Shock melting also trapped a component derived from the martian atmosphere, as revealed by stepped combustion–mass spectrometry. About 0.7 My ago, the sample was ejected from Mars and eventually landed on Earth in July 2011. The martian weathering features in Tissint described here are compatible with spacecraft observations on Mars, including those made by the NASA Viking landers, MER Spirit rover, and ESA's Mars Express orbiter (*5*, *21*–*23*).


**References and Notes**

1. D. D. Bogard, P. Johnson, *Science* **221**, 651 (1983).
2. R. H. Becker, R. O. Pepin, *Earth Planet. Sci. Lett.* **69**, 225 (1984).
3. A. H. Treiman, J. D. Gleason, D. D. Bogard, *Planet. Space Sci.* **48**, 1213 (2000).
4. G. Crozaz, M. Wadhwa, *Geochim. Cosmochim. Acta* **65**, 971 (2001).
5. Supplementary materials are available on *Science* Online.
6. P. Rochette *et al.*, *Meteorit. Planet. Sci.* **40**, 529 (2005).
7. A. O. Nier, M. B. McElroy, *J. Geophys. Res.* **82**, 4341 (1977).
8. I. A. Franchi, I. P. Wright, A. S. Sexton, C. T. Pillinger, *Meteorit. Planet. Sci.* **34**, 657 (1999).
9. J. Blichert-Toft, J. D. Gleason, P. Télouk, F. Albarède, *Earth Planet. Sci. Lett.* **173**, 25 (1999).
10. G. Dreibus *et al.*, *Meteorit. Planet. Sci.* **35**, A49 (2000).
11. J. A. Barrat, J. Blichert-Toft, R. W. Nesbitt, F. Keller, *Meteorit. Planet. Sci.* **36**, 23 (2001).
12. C. R. Neal, L. A. Taylor, J. C. Ely, J. C. Jain, M. A. Nazarov, *Lunar Planet. Sci.* **32**, 1671 (2001).
13. B. Marty, K. Hashizume, M. Chaussidon, R. Wieler, *Space Sci. Rev.* **106**, 175 (2003).
14. T. Owen *et al.*, *J. Geophys. Res.* **82**, 4635 (1977).
15. J.-A. Barrat *et al.*, *Geochim. Cosmochim. Acta* **66**, 3505 (2002).
16. V. Sautter *et al.*, *Earth Planet. Sci. Lett.* **195**, 223 (2002).
17. P. Beck *et al.*, *Geochim. Cosmochim. Acta* **70**, 2127 (2006).
18. D. W. Mittlefehldt, M. M. Lindstrom, *Geochim. Cosmochim. Acta* **67**, 1911 (2003).
19. M. N. Rao, L. E. Borg, D. S. McKay, S. J. Wentworth, *Geophys. Res. Lett.* **26**, 3265 (1999).
20. E. L. Walton, P. J. Jugo, C. D. K. Herd, M. Wilke, *Geochim. Cosmochim. Acta* **74**, 4829 (2010).
21. R. E. Arvidson, J. L. Gooding, H. J. Moore, *Rev. Geophys.* **27**, 39 (1989).
22. L. A. Haskin *et al.*, *Nature* **436**, 66 (2005).
23. A. Gendrin *et al.*, *Science* **307**, 1587 (2005).
24. J. A. Barrat *et al.*, *Geochim. Cosmochim. Acta* **83**, 79 (2012).
25. K. Marti, J. S. Kim, A. N. Thakur, T. J. McCoy, K. Keil, *Science* **267**, 1981 (1995).



**Acknowledgments:** We acknowledge D. N. Menegas and family for their generous donation enabling the acquisition of Tissint (BM.2012,M1), M. Aoudjehane for fieldwork, A. Aaranson for field information, J. Gibson for assistance with oxygen isotope analysis, L. Labenne for loan of a sample, and A. Irving for 400 mg of powdered sample. This study was funded at Hassan II University Casablanca, Faculté des Sciences Ain Chock, by Centre de Recherches Scientifiques et Techniques Morocco and CNRS France (Projet International de Coopération Scientifique, Sciences de l'Univers 01/10), and by Comité Mixte Inter Universitaire Franco-Marocain Volubilis (MA/11/252); CRPG Nancy, France, by the CNES, CNRS, and European Research Council under the European Community's Seventh Framework Programme (FP7/2007-2013 no. 267255); Université de Bretagne Occidentale–Institut Universitaire Européen de la Mer, Plouzané, France, by the Programme National de Planétologie, Institut National des Sciences de l'Univers; Open University, by Science and Technology Facilities Council grant to the Planetary and Space Sciences Discipline; and University of Alberta, by the Natural Sciences and Engineering Research Council of Canada (grant 261740-03).


**Supplementary Materials**

www.sciencemag.org/cgi/content/full/science.1224514/DC1
Materials and Methods
Supplementary Text
Figs. S1 to S11
Tables S1 to S13
References (*26*–*35*)


9 May 2012; accepted 25 September 2012
Published online 11 October 2012;
10.1126/science.1224514


# Development and Disintegration of Maya Political Systems in Response to Climate Change


**Douglas J. Kennett,[1]*† Sebastian F. M. Breitenbach,[2]* Valorie V. Aquino,[3] Yemane Asmerom,[4] Jaime Awe,[5] James U.L. Baldini,[6] Patrick Bartlein,[7] Brendan J. Culleton,[1] Claire Ebert,[1] Christopher Jazwa,[1] Martha J. Macri,[8] Norbert Marwan,[9] Victor Polyak,[4] Keith M. Prufer,[3] Harriet E. Ridley,[6] Harald Sodemann,[10] Bruce Winterhalder,[11] Gerald H. Haug[2]**



The role of climate change in the development and demise of Classic Maya civilization (300 to 1000 C.E.) remains controversial because of the absence of well-dated climate and archaeological sequences. We present a precisely dated subannual climate record for the past 2000 years from Yok Balum Cave, Belize. From comparison of this record with historical events compiled from well-dated stone monuments, we propose that anomalously high rainfall favored unprecedented population expansion and the proliferation of political centers between 440 and 660 C.E. This was followed by a drying trend between 660 and 1000 C.E. that triggered the balkanization of polities, increased warfare, and the asynchronous disintegration of polities, followed by population collapse in the context of an extended drought between 1020 and 1100 C.E.


The Classic Maya (300 to 1000 C.E.) left a remarkable historical record inscribed on well-dated stone monuments. Wars, marriages, and accessions of kings and queens are tied to long count calendar dates and correlate with specific days in the Christian calendar (Goodman-Thompson-Martinez correlation). The termination of this tradition between 800 and 1000 C.E. marks the widespread collapse of Classic Maya political systems. Multidecadal drought has been implicated, but remains controversial because of dating uncertainties and insufficient temporal resolution in paleoclimatic records. Lake sediments from the Yucatan Peninsula provided the first evidence of substantial drying in the Terminal Classic (*1*). However, disturbances to lake sediment sequences caused by prehistoric deforestation and agricultural expansion during the Classic Period complicate reproducing these results near the largest and most politically important Maya centers (such as Tikal and Caracol). Several studies more distant from the Maya lowlands (ML) support either relatively dry conditions or a series of droughts during the Terminal Classic (*2*–*5*), but the relevance of these records for the ML remains unclear (*6*).

Cave deposits in the ML show great promise for paleoclimatic reconstruction (*7*–*9*). The challenge lies in developing long, continuous records from rapidly growing stalagmites that can be dated precisely by using $^{234}$U-$^{230}$Th (U-Th). Here, we present a subannually resolved rainfall record from an exceptionally well-dated stalagmite collected from Yok Balum (YB) Cave in Belize (16°12'30.780" N, 89°4'24.420" W, 366 m above sea level) (*10*). YB cave is located 1.5 km from the Classic Period Maya site of Uxbenká. Three other important Maya centers (Pusilha, Lubaantun, Nim Li Punit) are within 30 km (fig. S1); Tikal and other major Classic Period population centers (such as Caracol, Copan, and Calakmul) are


[1]Department of Anthropology, Pennsylvania State University, University Park, PA 16802, USA. [2]Department of Earth Science, Eidgenössische Technische Hochschule (ETH), CH-8092 Zürich, Switzerland. [3]Department of Anthropology, University of New Mexico, Albuquerque, NM 87131, USA. [4]Department of Earth and Planetary Sciences, University of New Mexico, Albuquerque, NM 87131, USA. [5]Institute of Archaeology, National Institute of Culture and History, Belmopan, Belize. [6]Department of Earth Sciences, University of Durham, Durham DH1 3LE, UK. [7]Department of Geography, University of Oregon, Eugene, OR 97403, USA. [8]Department of Native American Studies, University of California, Davis, Davis, CA 95616, USA. [9]Potsdam Institute for Climate Impact Research, Post Office Box 60 12 03, 14412 Potsdam, Germany. [10]Institute for Atmospheric and Climate Science, ETH, CH-8092 Zürich, Switzerland. [11]Department of Anthropology, University of California, Davis, Davis, CA 95616, USA.

*These authors contributed equally to this work.
†To whom correspondence should be addressed. E-mail: djk23@psu.edu